Nuclear Materials and Energy 9 (2016) 394–398

Contents lists available at ScienceDirect

Nuclear Materials and Energy

journal homepage: www.elsevier.com/locate/nme

Development of yttrium-containing self-passivating tungsten alloys for future fusion power plants

T. Wegener[a,*], F. Klein[a], A. Litnovsky[a], M. Rasinski[a], J. Brinkmann[b], F. Koch[b], Ch. Linsmeier[a]

[a] Forschungszentrum Jülich GmbH, Institut für Energie- und Klimaforschung – Plasmaphysik, 52425 Jülich, Germany
[b] Max-Planck-Institut für Plasmaphysik, Boltzmannstr. 2, 85748 Garching, Germany

ARTICLE INFO

Article history:
Received 29 November 2015
Revised 26 June 2016
Accepted 8 July 2016
Available online 18 October 2016

Keywords:
W-based alloys
W-Cr-Y alloys
Oxide resistant W-Cr-Y alloys

ABSTRACT

Tungsten is a prime material candidate for the first wall of a future fusion reactor. In the case of a loss-of-coolant accident (LOCA) wall temperatures of about 1450 K could be reached lasting about 30–60 days due to nuclear decay heat. In the worst case scenario combining LOCA with air ingress, the formation and release of highly volatile and radioactive tungsten trioxide (WO_3) into the environment can occur. Smart self-passivating tungsten alloys preventing the formation of WO_3 can be a way to mitigate this release.

In this contribution we present the studies of a new yttrium-containing W-Cr-Y alloys. The extent up to which yttrium acts as an active element improving the adherence and stability of the protective Cr_2O_3 layer formed during oxidation is assessed. The approach is similar to the one taken for high-temperature steels where active elements stabilize the oxide layers at a substantially reduced thickness by changing the oxygen diffusion and improving the adherence of the protective oxide layer by e.g. avoiding of pores. Further, simulations on mobilized material for the case of a LOCA are developed. In addition, the loss of alloying elements during normal operation of a reactor is estimated. This is done by modelling a thermally activated diffusion, using a diffusion coefficient which is extrapolated from experimental data at higher values.

The oxidation behaviour of magnetron sputtered and therefore alloyed at the atomic level W-Cr-Y alloys is tested in a thermo-gravimetric facility. The isothermal oxidations are performed in a gas mixture, containing 20 kPa oxygen and 80 kPa argon under ambient pressure at temperatures of 1273 K and 1473 K, respectively. Experiments with W-Cr-Y show a parabolic oxidation rate of $k_p = 3 \cdot 10^{-6}\,\mathrm{mg^2\,cm^{-4}\,s^{-1}}$ which is more than five orders of magnitude lower than that of pure tungsten at 1273 K. Investigations using X-ray diffraction analysis and focused ion beam cross-sections in combination with scanning electron microscopy and energy dispersive X-ray spectroscopy are conducted. A protective Cr_2O_3 layer is detected on the surface with a thickness between 100 and 300 nm.

1. Introduction

Tungsten is one of the most promising candidate materials for the first wall in future fusion reactors having a high melting point, high thermal conductivity, low tritium retention and low erosion yield [1–3]. However, in case of a loss-of-coolant accident (LOCA), the temperature of the first wall armour made of tungsten could rise up to 1450 K within 20–40 days as shown in Fig. 1 [3]. In combination with a break of the vacuum vessel followed by air ingress, significant amounts of tungsten oxidise forming WO_3, which is mobilized by sublimation at temperatures of about 1170 K. At the highest predicted temperatures of around 1450 K an evaporation rate of $300\,\mathrm{m\,h^{-1}}$ is calculated assuming a 1000 m^2 of first wall surface [4], as shown in Fig. 2. In case of a reactor LOCA normally <50% of the elements typically found in the aerosols (like Ag, Re, W,...) are actually released into the environment [5].

Assuming a similar behaviour for a future fusion reactor, this would result in a mobilization rate of radioactive tungsten of the order of ~ 150 kg h^{-1}, which in turn equals an escaping activity of $\sim 7.5 \cdot 10^{16}\,\mathrm{Bq\,h^{-1}}$. This is an unacceptable value.

To prevent this release, self-passivating tungsten alloys with a new composition of about 12 wt.% chromium and 0.6 wt.% yttrium

* Corresponding author.
E-mail address: t.wegener@fz-juelich.de (T. Wegener).

http://dx.doi.org/10.1016/j.nme.2016.07.011

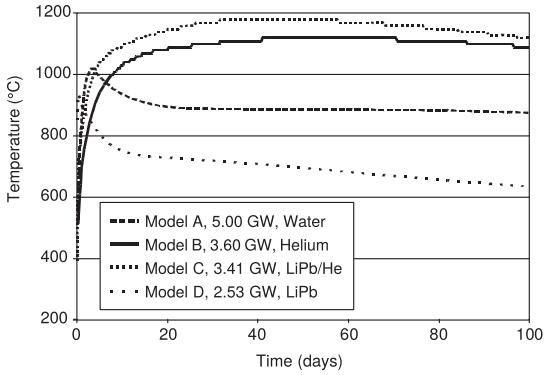

Fig. 1. Calculated temperature profiles after an accident with a total loss of all coolant [3].

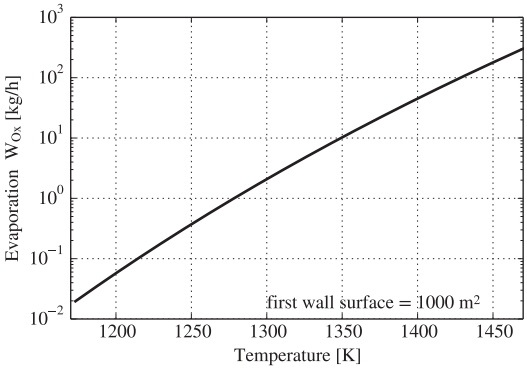

Fig. 2. Mass of tungsten lost by evaporating WO_3 in dependence of the temperature. This calculation assumes a LOCA combined with air ingress in a fusion reactor with a 1000 m^2 first wall, vapour pressure data is from ref. [6].

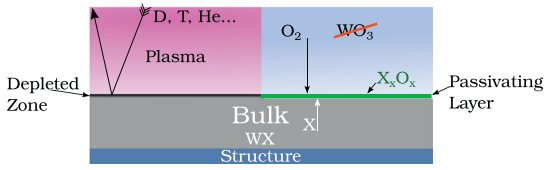

Fig. 3. Self-passivating tungsten alloys on the left side (a) during normal operation with a depleted zone of nearly pure tungsten on the plasma-facing surface and on the right side (b) in accidental condition with a protective passivating layer on the surface which prevents further oxidation of tungsten.

(W-12Cr-0.6Y) could be used. In case of a LOCA the chromium of the alloy forms a protective barrier layer of Cr_2O_3 on the surface and prevents further oxidation of the tungsten [7] as depicted on the right side in Fig. 3b. In regular plasma operation the alloyed chromium and yttrium are depleted in the first few nm of the plasma-facing surface by selective sputtering of alloying elements leading to a to nearly pure tungsten plasma-facing surface [8] as shown on the left side in Fig. 3a.

In the novel alloy, the active/reactive element yttrium is supposed to stabilize the passivating oxide layer similar as reported for the W-Cr-Y_2O_3 system [9]. In literature three main possible ways on how active elements work are discussed. Firstly, they are thought to form pegs, which act as a connection between the oxide and the alloy as shown in the Fig. 4a [10–12]. Secondly active elements alter the diffusion, so that the oxide layer grows from the metal surface, avoiding pores as shown in Fig. 4b [10]. Thirdly they react with impurities like S, C or P as illustrated in Fig. 4c. Otherwise, these impurities destabilize the oxide layer [11]. It is stated that yttrium is reducing the thickness of the protective oxide layer [13], leading to more efficient self-passivation. Apart from

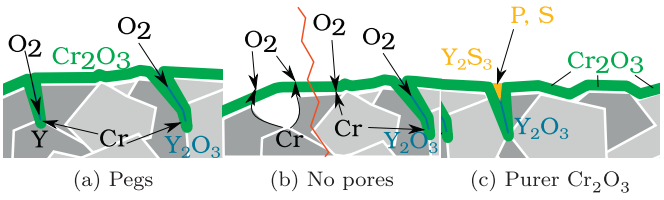

Fig. 4. Ways of how yttrium effects the adhesion and stability of the oxide layer. (a) Pegs are improving the adhesion. (b) yttrium alters transport mechanism through the oxide, avoiding of pores. (c) Reaction of yttrium with impurity's, improves the purity of the Cr_2O_3 scale.

these studies, mostly concentrating on steels and nickel based alloys, several studies were already published investigating the possibility to improve the oxidation behaviour of tungsten by adding various elements like Si, Cr, Ti, Ta, Nb and Zr to name a few [9,14–20]. Also, Y was part of the elements which were screened in one of the studies. In this study on thin films W-14Cr-2Ti and W-18Cr-2Ti showed the best results on oxidation behaviour [7]. Nevertheless, this could be related to the near to optimum chromium content (as shown in Fig. 8 of $\geq$ 12 wt.%) of the investigated W-Cr-Ti alloys in combination with the low chromium and high yttrium content in the investigated W-7Y-3Cr alloy. These studies and others already indicate the beneficial effects of Cr as main passivating agent for W which is also used in this study.

For the oxidation behaviour two different models are used:

$$\left(\frac{\Delta m}{A}\right) \propto k_l \cdot t \tag{1}$$

Where Δm is the change of mass while oxidation, A the surface area of the specimen, and t the time.

Linear oxidation behaviour (Eq. (1)) takes place where the oxygen adsorption is the rate determining step, normally this is the case where the metal builds a porous oxide layer. Furthermore, the velocity remains constant over time and is given as k_l the linear oxidation constant for a certain temperature [10]. Pure tungsten exhibits such a linear oxidation behaviour for the temperature ranges and time intervals under consideration.

$$\left(\frac{\Delta m}{A}\right)^2 \propto k_p \cdot t \tag{2}$$

Parabolic oxidation behaviour (Eq. (2)) occurs when a metal forms a stable protective oxide layer on the surface, which decelerates the oxidation. After formation of a continuous oxide layer, the diffusion of reactants (cations and/or anions) through the growing oxide layer gets the rate determining step [10]. The resulting parabolic oxidation constant is given as k_p. In this study the beneficial effects of yttrium addition to the binary W-Cr alloys are further investigated.

2. Theoretical assessment

A key question on the feasibility of self-passivating tungsten alloys is being how the material composition of the first wall is changed during regular plasma operation and if the beneficial properties are preserved till the LOCA. To approach this issue a one-dimensional diffusion model is used with the boundary condition.

$$c(x = 0) = c(x = d) = 0$$

Hence, the concentration c of the considered element on the surface of a layer is zero [21]. The concentration of the observed element depends on the time t and the position relative to the surface x, d is the thickness of a layer and c_0 represents the initial

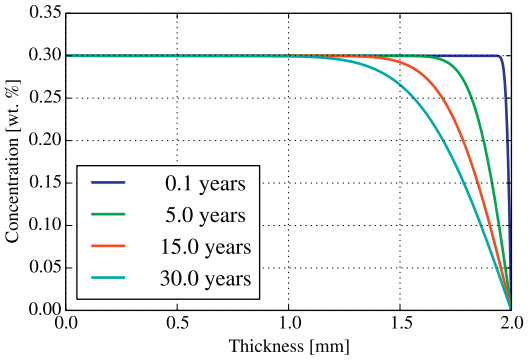

Fig. 5. Yttrium loss over sputtering time in normal reactor operation in the first 2 mm of the first wall. Diffusion coefficients are taken from [22].

concentration. A way to solve the problem is a Fourier development depicted in Eq. (3) from [21]. This creates an axially symmetrical concentration profile. In this case only one side of the profile is considered, since only one side of the layer is facing the plasma. The tungsten layer thickness is defined as $d/2 = 2$ mm.

$$c(x,t) = \sum_{n=1,3,5\ldots}^{\infty} \frac{4c_0}{n\pi} \cdot \sin\left(\frac{n\pi}{d}x\right) \exp\left(-\left(\frac{n\pi}{d}\right)^2 Dt\right) \tag{3}$$

This provides insight into the time evolution of the spatial variation of the concentration considering the influence of preferential sputtering on the surface. The result is shown in Fig. 5. The yttrium concentration decreases relatively slow over a period of about 5–30 years at a temperature of 1473 K (which is approximately twice as high as stated in [4]).

For chromium the same calculation is performed, with the result of much longer time scales of several thousand years untill a significant loss of chromium is observed. This idealized simulation shows that the loss of alloying elements due to diffusion and sputtering is small. However, further experimental investigations are needed to verify the applied approximations and to perform the corresponding modelling.

3. Material and methods

The samples for this study were produced by magnetron sputtering. Tungsten, chromium and yttrium targets operate simultaneously [14]. For the deposition process chromium (99.95 wt.%) and tungsten (99.95 wt.%) targets were operated by a DC power supply at 180–275 W and 420–500 W. The yttrium (99.9 wt.%) target was operated with a RF power supply at 140–330 W to achieve reliable deposition rates even at low yttrium concentrations in the alloys. The alloys were deposited on sapphire substrates, as recommended in ref. [14]. They have a diameter of 12 mm and 0.5 mm thickness, the deposited films are $\sim 3.5\ \mu$m thick. After the deposition, the alloying elements were distributed at the atomistic level throughout the entire thickness of the alloy. The thin-films have a grain size in range 50–200 nm with a columnar like and dense structure without any pores.

Several samples were prepared in multiple, independent processes using the aforementioned magnetron sputtering device. The obtained elemental composition was determined separately for each process by Wavelength-Dispersive X-Ray Fluorescence (WDXRF) using a sequential x-ray spectrometer (PW2404, PHILIPS). As a result, the samples contained W with 8–13.5 wt.% Cr and 0.4–1.7 wt.% Y which were used for experiments on the influence of the elemental composition and the temperature.

Oxidation testing is performed in a thermo-gravimetric facility (TAG 16 from Setaram). It controls atmosphere and temperature while measuring the mass change of the sample over time. The

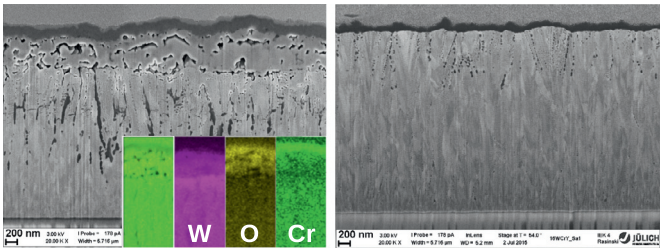

(a) Binary W-Cr (b) Ternary W-Cr-Y

Fig. 6. SEM images of FIB prepared cross-section of the binary W-Cr (a) and the tenary W-Cr-Y (b) alloys.

oxidation is performed at isothermal conditions with constant flow of the gas mixture Ar-20 vol.%O_2 with 20 ml minm^{-1} of 20 kPa O_2 and 80 kPa Ar. In order to compare with earlier results from [7].

Before and after oxidation several analytical techniques like Scanning Electron Microscopy (SEM) in combination with Focused Ion Beam (FIB) cross-sectioning (Carl Zeiss CrossBeam XB 540), X-Ray Diffraction (XRD) (D8 from Bruker), Energy Dispersive X-ray spectroscopy (EDX) were employed to examine the microstructure, homogeneity, elemental composition and morphology of the alloys and the oxides [23,24].

4. Results

4.1. Oxidation at 1273 K

In this section the oxidation behaviour of W-Cr-Y and W-Cr is compared. In the Fig. 6 a comparison of the micro-structure after oxidation at 1273 K for 15 min in SEM image of a FIB cross-section combined with EDX analyses of the alloys are shown. In the binary W-Cr alloy cross-section the top layer consists of Cr_2O_3, the layer below has a porous micro-structure consisting of $W_xCr_yO_z$, which was supported by XRD measurements. In addition, a chromium depletion is visible in the EDX of Fig. 6a. In the bulk, dark spots are visible which are Cr_2O_3 precipitates as confirmed by EDX mapping results.

The top Cr_2O_3 layer in the W-Cr-Y system (Fig. 6b) has a thickness of $0.12 \pm 0.03\ \mu$m. In comparison it is $0.20 \pm 0.04\ \mu$m thick for the W-Cr system in Fig. 6a. Measurements with different oxidation times show that in the W-Cr-Y system the Cr_2O_3 layer grows continuously with time. In the W-Cr-Y system mixed oxides are neither visible in the SEM image 6b, nor in the XRD measurement. The amount of pores and the formation of Cr_2O_3 precipitates is suppressed in the W-Cr-Y system. The oxidation performance is further investigated by the dynamic weight gain during the oxidation, which is measured in a thermogravimetric system. The results for a binary W-10.3 wt.%Cr alloy and a ternary W-10.4 wt.%Cr-1.2 wt.%Y alloy at 1273 K in Ar-20 vol.%O_2 are shown in Fig. 7.

In case of W-Cr a transition from parabolic Eq. (2) to linear oxidation Eq. (1) behaviour is visible after about 6 min. W-Cr-Y shows parabolic oxidaiton behaviour for about two hours. The integrated mass gain is reduced by a factor of four during the first 15 min.

In order to investigate the influence of the chromium and yttrium content on the oxidation behaviour in the W-Cr-Y system, two experiment series were conducted, each with a variation of the chromium or yttrium concentration while the concentration of the other alloying element was kept approximately constant. Fig. 8 shows the mass change with respect to time during oxidation. For increasing chromium concentrations of up to 11.4 wt.% the mass gain per time decreases. The transition from slow, parabolic oxidation to faster, linear oxidation behaviour (both explained in Section 1) occurs earlier for lower chromium concentrations. Beyond 12 wt.% chromium mass gain slightly increases again. The transition point from parabolic to linear oxidation behaviour, is

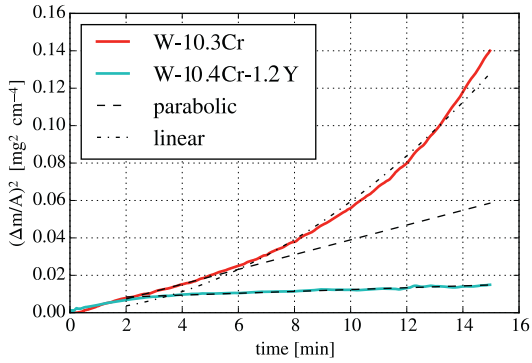

Fig. 7. Quadratic mass increase normalized to specimen surface area as a function of the oxidation time of a W-10.4Cr-1.2Y and W-10.3Cr alloy at 1273 K in Ar-20 vol.%O_2.

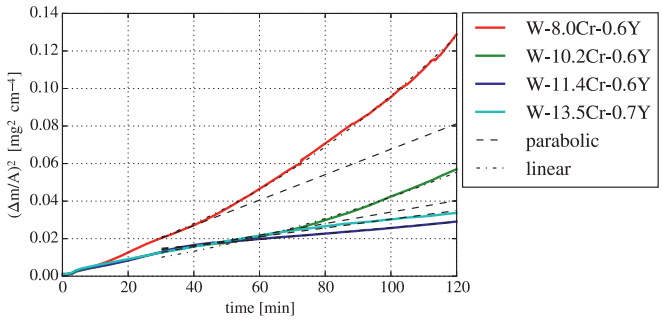

Fig. 8. Quadratic mass increase normalized to specimen surface area as a function of the oxidation time for samples with different chromium concentrations and approximately constant yttrium concentrations at 1273 K in Ar-20 vol.%O_2.

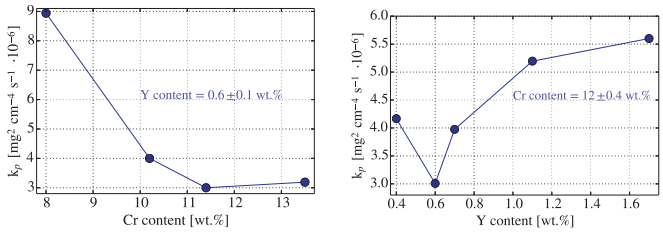

(a) Variation of Cr content. (b) Variation of Y content.

Fig. 9. Oxidation rate constant against the variation of yttrium or chromium concentrations with the concentrations of the other alloying element kept approximately constant.

not found within the chosen oxidation time of 2 h for 11.4 and 13.5 wt.% of chromium.

Shown in Fig. 9a, a parabolic fit was applied through the mass gain in the time range, where it follows a parabolic dependence on oxidation time. Results of these fits are shown in Fig. 9a where the dependence of the oxidation rate k_p on the chromium concentration is plotted. The same investigation was done to evaluate the optimum yttrium concentration. The result is shown in Fig. 9b.

4.2. Oxidation at 1473 K

Experiments at 1473 K are conducted due to the encouraging self-passivation behaviour of the W-Cr-Y alloy at 1273 K and the need to approach the highest predicted fusion reactor wall temperatures in case of a LOCA. It is apparent that evaporation of WO_3 becomes dominant at these temperatures, when failure of the passivating Cr_2O_3 layer occurs (see to Fig. 2). In Fig. 10 the oxidation of W-Cr, W-Cr-Y at 1473 K and for comparison W-Cr-Y at 1273 K are plotted. Except for W-11.4Cr-0.6Y the samples are exposed to

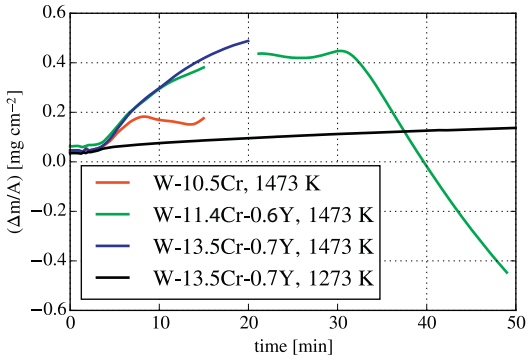

Fig. 10. Oxidation of W-Cr, W-Cr-Y at 1473 K, and W-Cr-Y at 1273 K. All the samples are exposed to Ar-20 vol.%O_2 for the entire measurement time, except for W-11.4Cr-0.6Y (green curve) which is exposed to Ar-20 vol.%O_2 for 15 min, afterwards it is held in low oxygen Ar atmosphere. The flush of Ar, which is cleaning the atmosphere, is not plotted. (For interpretation of the references to colour in this figure legend, the reader is referred to the web version of this article.)

Ar-20 vol.%O_2 for the entire measurement range. W-11.4Cr-0.6Y is exposed to Ar-20 vol.%O_2 for 15 min, afterwards it is kept in low oxygen Ar atmosphere. The disturbance of the weight signal, during the furnace is flushed out with Ar is not displayed. This results in the time gap of about 4 min.

5. Discussion

5.1. W-Cr compared to W-Cr-Y

The observations in Figs. 6 and 7 indicate that yttrium supports the formation a continuously growing layer of Cr_2O_3, which is dense enough to be an efficient diffusion barrier for oxygen. This is indicated by the strong reduction in mass gain over time compared to the W-Cr alloy shown in Fig. 7. Further, yttrium suppresses the formation of mixed oxides and pores under the protective Cr_2O_3 layer which is visible in the Fig. 6b. The absence of pores and mixed oxides reduces the probability of scale failures and layer spalling as the connecting area of the oxide metal interface and so the adhesion increases. That also fits to the observation of the earlier transition from slow parabolic to fast linear oxidation in case of the W-Cr alloy after only 6 min (see Fig. 7). Since, a failure of the protective Cr_2O_3 layer leads to a direct path for oxygen to the metal surface and so to a faster oxidation. In comparison, the same transition from parabolic to linear oxidation behaviour takes $\sim$ 2 h in case of the ternary W-Cr-Y, because of the benefits of yttrium like the improved adhesion discussed above.

5.2. Influence of chromium and yttrium content on oxidation constant

In Fig. 8a shift of the transition from parabolic to linear oxidation behaviour with increasing chromium concentration is occurring. A possible explanation for this shift is that the concentration of chromium has a minimum limit for the formation of a protective Cr_2O_3 layer in case of yttrium-containing alloy. This minimum limit is calculated by taking the total weight gain at the transition to the linear oxidation behaviour in Fig. 8. This weight gain is assumed to be stoichiometric Cr_2O_3 which makes it possible to calculate the amount of chromium consumed till the linear oxidation starts. When this consumed chromium is subtracted from the initial amount of chromium in the thin alloy layer of 3.5 μm, one comes up with values of about $\sim$ 8 wt. % as a minimum limit of chromium to form a protective Cr_2O_3 layer.

With increasing chromium concentration in the alloy the oxidation rate decreases down to 11.4 wt.% (see Fig. 9a). However,

an increase to higher concentrations of chromium do not necessarily lead to better passivation behaviour, as the solubility at 1273 K is limited to only a few weight-percent as reported by [25]. Since, chromium being present in concentrations above the solubility threshold in the alloys, due to the atomic disperse nature of sputter deposited films, the chromium will segregate due to thermally induced diffusion leading to precipitates. This precipitates are visible by the gray spots in the lower part of the alloy layer in Fig. 6b. Furthermore, an additional supply of oxygen leads to oxidation and agglomeration of the Cr_2O_3, visible as the dark spots at the higher part of the thin film cross-section directly under the protective Cr_2O_3 layer in the Figs. 6. The amount of Cr_2O_3 implies that the total amount of elemental chromium in the alloy decreases by about 33% during the chosen oxidation time. Therefore, a thin film system is not suitable to investigate the long-term oxidation performance of the initially manufactured system.

For an application as a plasma-facing material of the self-passivating tungsten alloys, chromium is only required for accidental scenarios and under normal operation the chromium concentration should be kept as low as possible. Therefore, we can conclude that the optimum for the chromium concentration is about $\sim$ 12 wt.% chromium.

The yttrium concentration has a strong influence on the oxidation rates (see Fig. 9b). The optimum yttrium concentration is about 0.6 wt.%. This could be partly explained by the discussion in Section 5.1. However, the benefits are reduced when the concentration is increased or decreased. The strong dependence on the actual concentration of yttrium in the system, needs further investigation.

5.3. Oxidation at 1473 K

For the binary W-Cr alloy the oxidation at 1473 K leads to a rapid weight gain. After 5 min the evaporation gets comparable in mass flow to the oxidation and later becomes the dominant process. This leads first to a reduced weight gain with time followed by a weight loss (see Fig. 10), while the oxidation was still in process indicated by the small weight gain at this point in time. At 1473 K, the W-Cr-Y system suppresses evaporation of WO_3 over time period of about 20 min. In a second experiment with W-Cr-Y it is shown that (see the green curve in Fig. 10), after 15 min oxidation, keeping the temperature for another 15 min, in this time evaporation levels the mass gain by oxidation in atmosphere with reduced oxygen content. However, then a rapid weight loss occurs which is in the same order of magnitude as the predicted evaporation of pure WO_3. The failure of the protective oxide layer may associated with reaching the minimum limit of chromium concentration to further form a protective Cr_2O_3 layer.

6. Conclusions

In this study the losses of alloy elements by diffusion in combination with sputtering on the first wall are predicted for normal operation of a fusion reactor. It is found to be sufficiently small for a first wall lifetime of about 10 years. It was shown that yttrium improves the self-passivation of the investigated W-Cr-Y alloys, but too much yttrium reduces the benefits. The effects of yttrium are the suppression of mixed oxides and pores. It reduces the oxidation rates by at least one order of magnitude compared to the W-Cr system. The optimum composition found in this study and so the starting point for the production of bulk material is of W-$\sim$ 12 wt.%Cr-0.6 wt.%Y. The oxidation stability is increased also at 1473 K for the W-Cr-Y system, compared to that of the binary W-Cr as evaporation gets dominant after a four times longer time period for the investigated yttrium-containing thin films. The beneficial effects of yttrium on the W-Cr-Y system were clearly demonstrated. A complete picture of the mechanisms induced by yttrium could not be drawn from studies of model thin films and will be in focus of future investigations.

Acknowledgments

The authors want to acknowledge support by Alexis Terra with the magnetron sputter device. Further we want to thank Dr. Timo Dittmar for providing insight into the programming and plotting of IPython [26]. This work has been carried out within the framework of the EUROfusion Consortium and has received funding from the Euratom research and training programme 2014–2018 under grant agreement No 633053. The views and opinions expressed herein do not necessarily reflect those of the European Commission.

References

[1] H. Bolt, V. Barabash, G. Federici, J. Linke, A. Loarte, J. Roth, K. Sato, Plasma facing and high heat flux materials – needs for ITER and beyond, J. Nuclear Mater. 307 - 311, Part 1 (2002) 43–52.
[2] G. Federici, C. Skinner, J. Brooks, J. Coad, C. Grisolia, A. Haasz, A. Hassanein, V. Philipps, C. Pitcher, J. Roth, W. Wampler, D. Whyte, Plasma-material interactions in current tokamaks and their implications for next step fusion reactors, Nuclear Fusion 41 (12) (2001) 1967.
[3] D. Maisonnier, P.I. Cook, R.A. Sardain, L.D. Pace, R. Forrest, L. Giancarli, S. Hermsmeyer, P. Norajitra, N. Taylor, D. Ward, A concetptual study of commercial fusion power plants, Final Report of the European Fusion Power Plant Conceptual Study (PPCS), EFDA, 2005. EFDA(05)-27/4.10.
[4] Y. Igitkhanov, B. Bazylev, I. Landman, R. Fetzer, Design strategy for the pfc in demo reactor, Kit Scientific Reports (Report-Nr. KIT-SR 7637) (2013).
[5] M. Schwarz, G. Hache, P. von der Hardt, Phebus fp: a severe accident research programme for current and advanced light water reactors, Nuclear Eng. Des. 187 (1) (1999) 47–69.
[6] J. D'Ans, W. Heiland, P. Hertel, Taschenbuch fuer Chemiker und Physiker: Band I Physikalisch-chemische Daten, 4., Springer, 1992.
[7] F. Koch, J. Brinkmann, S. Lindig, T.P. Mishra, C. Linsmeier, Oxidation behaviour of silicon-free tungsten alloys for use as the first wall material, Physica Scripta 2011 (T145) (2011) 014019.
[8] W.E. et al., Atomic and Plasma-Material Interaction Data for Fusion, 7b, IAEA, Vienna, 2001.
[9] S. Telu, R. Mitra, S.K. Pabi, Effect of Y_2O_3 addition on oxidation behavior of W-Cr alloys, Metallurgical Mater. Trans. A 46 (12) (2015) 5909–5919.
[10] N. Birks, G. Meier, F. Pettit, Introduction to the High-Temperature Oxidation of Metals, Cambridge University Press, 2006.
[11] R. Buergel, H.J. Maier, T. Niendorf, Handbuch Hochtemperatur-Werkstofftechnik, PRAXIS, 2011.
[12] R. Mevrel, Cyclic oxidation of high-temperature alloys, J. Mater. Sci. Technol. (1987).
[13] K. Przybylski, A.J. Garratt-Reed, G.J. Yurek, Grain boundary segregation of yttrium in chromia scales, J. Electrochem. Soc. 135 (2) (1988) 509–517.
[14] F. Koch, S. Koeppl, H. Bolt, Self passivating W-based alloys as plasma-facing material, J. Nuclear Mater. 386 - 388 (2009) 572–574.
[15] P. López-Ruiz, N. Ordás, S. Lindig, F. Koch, I. Iturriza, C. García-Rosales, Self--passivating bulk tungsten-based alloys manufactured by powder metallurgy, Physica Scripta 2011 (T145) (2011) 014–018.
[16] P. López-Ruiz, N. Ordás, I. Iturriza, M. Walter, E. Gaganidze, S. Lindig, F. Koch, C. García-Rosales, Powder metallurgical processing of self-passivating tungsten alloys for fusion first wall application, J. Nuclear Mater. 442 (2013) 219–224.
[17] S. Telu, V. Karthik, R. Mita, S.K. Pabi, Effect of 10 at.% Nb addition on sintering and high temperature oxidation of $W_{0.5}Cr_{0.5}$ alloy, Mater. Sci. Forum 710 (2012) 308–313.
[18] S. Telu, A. Patra, M. Sankaranarayana, R. Mitra, S. Pabi, Microstructure and cyclic oxidation behavior of W-Cr alloys prepared by sintering of mechanically alloyed nanocrystalline powders, Int. J. Refractory Metals Hard Mater. 36 (0) (2013) 191–203.
[19] S. Espevik, R. Rapp, P. Daniel, J. Hirth, Oxidation of Ni-Cr-W ternary alloys, Oxidation of Metals 14 (2) (1980) 85—108. 24 Seiten, 18 Quellen %9 Journal.
[20] T. Weissgaerber, B. Kloeden, B. Kieback, Self-passivating tungsten alloys, Powder Metallurgy World Congress Exhibition 3 (2010) 377–383. ISBN: 978-1-899072-12-5.
[21] H.G. Zachmann, Mathematik fuer Chemiker, 4, 4. edition, VCH, 1990.
[22] G. Neumann, C. Tuijn, Chapter 6 self-diffusion and impurity diffusion in group vi metals, in: G. Neumann, C. Tuijn (Eds.), Self-Diffusion and Impurity Diffusion in Pure Metals: Handbook of Experimental Data, Pergamon Materials Series, 14, Pergamon, 2008, pp. 239–257.
[23] J. Goldstein, Scanning Electron Microscopy and X-ray Microanalysis: Third Edition, Scanning Electron Microscopy and X-ray Microanalysis, Springer US, 2003.
[24] S. Reyntjens, R. Puers, A review of focused ion beam applications in microsystem technology, J. Micromech. Microeng. 11 (4) (2001) 287.
[25] P. Villars, Cr-W binary phase diagram 0-100 at., Springer Mater. (2014).
[26] F. Perez, B.E. Granger, IPython: a system for interactive scientific computing, Comput. Sci. Eng. 9 (3) (2007) 21–29.